Offset-dependent tuning effects of thin layers and a model study of two layers

Hai-man Chung and Don C. Lawton

ABSTRACT

The offset-dependent amplitude of a single low-velocity thin layer embedded in a homogeneous thick layer is studied. It is found that for the P-wave maximum peak amplitude, the change in amplitude as a result of a change in Poisson's Ratio is adversely affected by the effects of offset-dependent tuning. In the absence of the tuning effects, the P-wave amplitude increases by more than 90% for some offsets as Poisson's Ratio for the thin layer changes from 0.25 to 0.1. But with tuning, the percentage drops to less than 20%. For the PS-wave maximum peak amplitude, the effects of tuning are less severe.

The study of two-layer model indicates that the tuning thickness for the upper layer remains at 1/4 of the predominant wavelength, regardless of the thickness of the lower layer. A plot of the trough to peak amplitude appears to be more diagnostic of the thickness of the lower layer than the plot of absolute maximum amplitude of the reflected composite wavelet. The instantaneous frequency also appears to be useful to differentiate the subtle waveform changes introduced by varying the thickness of the lower layer.

OFFSET-DEPENDENT TUNING EFFECTS

In the Western Canadian Sedimentary Basin, the geological formations comprising the Cretaceous period are composed of many thin clastic layers. In the last decade or so, a great deal of interest has been generated by the potential use of shear wave and AVO (amplitude variation with offset) effects to detect the presence of gas in clastic layers, as discussed by Ostrander (1984), Ensley (1984), Wren (1984), McCormack et al (1984), Jain (1987), and Robertson et al (1985). However, if the layers are thin, i.e. below the tuning thickness, the effects of offset-dependent tuning could lead to AVO effects that would otherwise be absent, as discussed by Chung and Lawton (1990). Conversely, there are also situations where the effects of offset-dependent tuning overwhelm the AVO effects due to lateral change of Poisson's Ratio. In either situation, using inversion technique to deduce Poisson's Ratio from the offset-dependent amplitudes is at best erroneous. The question to which we seek an answer is how much does offset-dependent tuning effects affect the amplitudes.

Model A (Fig. 1a) and Model B (Fig. 1b) are two simple models we use to answer that question. The only difference between the two models is that Model A has one interface and Model B has two interfaces. Consequently, Model A leads to no offset-dependent tuning effects in the resulting synthetic seismograms whereas Model B does. The velocities chosen reflect the velocities of some of the Cretaceous clastic layers in Southern Alberta, and the densities are derived from the

velocities using Gardner's equation (Gardner, 1974). Shot records are generated for each model, using a Ricker zero-phase 31 Hz wavelet, with Poisson's Ratio equal to 0.25 and 0.1 for the thin layer, i.e. two synthetic seismograms for each model. Trace spacing is 50 m with 60 traces spanning the 3000 m spread. Poisson's Ratios for the overlying and underlying halfspaces are kept constant at 0.25. The procedure is repeated for Model B for two thicknesses, i.e. 5 m and 10 m. Note that for the velocities and the wavelet chosen, the predominant wavelength λ_d in the thin bed in Model B is 73.9 m, so that a thickness of 10 m is only about 0.76 m larger than the (1/8) λ_d value. The models are run with the Outrider package where the exact Zoeppritz-equations are solved, and transmission coefficients are applied but omitting the effects of spherical divergence. All the resulting synthetic seismograms are shown in Figures 2a to 2f. Both the P-wave and the PS-wave total displacements are studied. Also note that, the models are set up in such a way that there is no critical angle involved in ray-tracing both Model A and Model B. In Figures 2a to 2f, it is evident that the amplitude change for the P-wave as Poisson's Ratio changes from 0.25 to 0.1 is considerably larger in the case without tuning effects compared to the cases with tuning effects. For the PS-wave, it is less evident how the amplitude change compares among the three cases. Figures 3a and 3b show the quantitative results of the study of the maximum peak amplitude of the reflected composite wavelet. All curves are calculated according to the following equation:

$$\% \text{ change in amplitude} = \frac{\text{amp } (\sigma = 0.25) - \text{amp } (\sigma = 0.1)}{\text{amp } (\sigma = 0.25)} \times 100\%$$

The curves D_r are the results for Model A. They represent the percentage change in amplitude solely as a result of a change in Poisson's Ratio without any tuning effects. The curves D_5 and D_{10} are for Model B for bed thicknesses 5 m and 10 m, respectively. They include both the effects of a change of Poisson's Ratio and offset-depending tuning. Let us first discuss the P-wave results.

For the P-wave (Fig. 3a), comparing the D_r curve with the D_5 and D_{10} curves, it is evident that the offset-dependent tuning effects have reduced Poisson's Ratio effect dramatically. Except for the very near offsets, the amplitude percentage increase without tuning as represented by D_r is considerably higher than that of D_5 and D_{10}. In particular, at the incident angle of around 55°, Poisson's Ratio change leads to an amplitude increase of over 90%. But this percentage is reduced to only about 20% for D_5 and 40% for D_{10}. From these curves, one could conclude that for beds less than (1/8) λ_d, which is slightly larger than the (1.36/10) λ_d value for the 10 m thickness, offset-dependent tuning effect negates true AVO effect.

For the PS-wave (Fig. 3b), the percentage change in amplitude is a decrease. The results are significantly different from that of the P-wave. For incident angles up to about 70°, the offset-dependent tuning effects enhance the effect of Poisson's Ratio change. In other words, the offset-dependent tuning effects make true AVO effect stronger than it really is. However, the differences between the two effects for a large incident angle range is much smaller than that of the P-wave. This is to be expected, since the S-wave velocity is slower than the P-wave velocity, resulting in a larger time thickness for the thin bed in Model B, and hence less tuning effects. The difference is, in fact, only a few units in percentage and implies that AVO effects due to a lateral change in Poisson's Ratio could probably be more reliably observed on S-wave data up to a value of 70° for the incident angle, assuming that the S-wave data has the same frequency content as the P-wave. Another interesting feature of the PS-wave is that the three curves D_r, D_5 and D_{10} intersect each other at different incident angles. Since the tuning effect of two wavelets depends on both their time

separation and relative amplitudes, one has to perform detail analyses of the traveltimes and offset-dependent reflection coefficients as a function of the incident angle for the three cases in order to understand the occurrence of these intersections.

A MODEL STUDY OF TWO LAYERS

(a) Amplitude

In the last two decades or so, there have been progressive studies on the reflection properties of a single thin bed embedded in a thick homogeneous bed. Papers by Widess (1973), Koefoed and de Voogd (1980), Kallweit and Wood (1982), de Voogd and Rooijen (1983), Robertson & Nogami (1984), Lange and Almoghrabi, and Gochioco (1991) are all good examples. While their results offer valuable insight into the stratigraphic interpretation of thin beds, there has been very little discussion concerning the reflection properties of more than one thin bed, i.e. two or three thin layers stacked together and embedded in a thick homogeneous layer. The paper by Meissner and Meixner (1969) discussed the interference pattern of two thin layers, but the discussion is somewhat qualitative and is restricted to two examples. Our intention is to run five or six two-layer models that correspond to some geological situations. By analyzing the amplitudes, frequencies and phases of the composite reflected wavelets from these models, we will seek some commonalities among them in terms of both useful characteristics that could be used for interpreting two thin layers as well as some pitfalls in the interpretation. For this paper, we will only discuss the amplitude and phase study of one of the models, since we are still in the process of running and analyzing other models and their results.

Figure 4 shows the two-layer model 2M1T. The velocities are chosen to reflect a coarsening upward sequence such as a channel facies. The upper thin wedge could represent the prospective porous sand of an upper channel facies, while the lower thin bed could represent the silty, non-porous lower channel facies. The wedge thickens from 1 m to 51 m, and the trace spacing in the corresponding synthetic seismograms is set up so that trace 1 corresponds to the wedge thickness of 1 m, trace 2 2 m, trace 3 3 m, and so on. A Ricker zero-phase 31 Hz wavelet is used to generate the synthetic seismograms, and only vertical incidence is considered, with transmission coefficients applied. The procedure is repeated five times with six different thicknesses for the thin layer underlying the wedge; the thicknesses are 0 m, 5 m, 10 m, 15 m, 20 m and 25 m.

Figures 5a to 5f show the corresponding synthetic seismograms. On the top of each seismogram, the thickness of the thin layer underlying the wedge is indicated. Marked also are the trace positions at which the wedge thicknesses are equal to 1/8 and (1/4) λ_d, i.e. 9.24 m and 18.48 m, respectively. Note that our zone of interest is where the wedge thickness is below the tuning thickness, i.e. below the thickness equal to (1/4) λ_d. If we compare the amplitude variations of the six seismograms in the zone of interest, they all appear to decrease gradually as the wedge thins. Given anyone of the six seismograms alone, one would not be able to identify which case it is based on amplitude alone. Figure 6 is a plot of the absolute values of the troughs of the reflected composite wavelets. Since the six curves for the six cases somewhat overlap each other, and the transition from the 0 m curve to the 25 m curve is gradual, for clarity, we have chosen to plot only 3 curves, namely, the curves for 0 m, 10 m and 25 m.

There are two interesting observations. The first observation is that tuning, i.e. maximum amplitude, is observed for all six cases at about 19 m, which is where the wedge thickness is approximately equal to $(1/4)\lambda_d$. The second observation is that for wedge thicknesses up to $(1/8)\lambda_d$, the amplitude plot versus wedge thickness is a straight line for the 0 m, 5 m and 10 m cases, but is a curve for the 15 m, 20 m and 25 m cases. Thus, while one cannot differentiate the six cases by their tuning thicknesses, their amplitude behaviour for wedge thicknesses below $(1/8)\lambda_d$ would allow some approximate prediction of the thickness of the underlying thin layer.

Another interesting amplitude property is the trough to peak ratio for the reflected composite wavelet. Figure 7 shows the plots of the ratio of the absolute values of the troughs to the value of the peaks for the same three cases shown in Figure 6. Here, one can see some significant differences between the three cases. As a general trend, the trough to peak ratio curves increases in value not only as the wedge thickness increases, but increases even more dramatically as the thickness of the underlying layer increases. Another interesting feature is that from the 5 m case to the 25 m case, the curve slowly changes from a rather flat curve to a curve with two prominent inflection points, reflecting the cyclical nature of the interference pattern of the input wavelet. These plots also suggest their possible use to obtain some information about the relationship between the thicknesses of two thin layers which represent a coarsening upward sequence.

(b) Complex Attributes

The use of complex attributes for geophysical application was introduced by Taner et al (1977, 1979) in the late seventies. Robertson and Nogami (1984) also discussed their usage for thin-bed delineation. However, their use in exploration has not been very widespread, judging from the scarce published literature on the subject. Our purpose of using complex attributes is two-fold. Firstly, complex attributes offer the advantage of separating the amplitude information from the phase and frequency information. Thus, any subtle changes would be better defined with the instantaneous frequency and the instantaneous phase than with the conventional seismic data. We are exploring the possibility of using the instantaneous phase and frequency to detect any subtle waveform changes due to a change in the thickness of a thin bed, as well as to differentiate the different reflected composite wavelets from different geological models of thin layers. Secondly, we want to learn more about the properties of complex attributes in general, but especially in their application to thin-bed delineation.

Figures 8a to 8f are the corresponding instantaneous amplitude plots for the synthetic seismograms in Figure 2. In the zone of interest [0 m to $(1/4)\lambda_d$ with respect to the wedge], they all appear similar to one another. Tuning occurs at $(1/4)\lambda_d$ for all six cases. This agrees with the amplitude plot in Figure 6. Note that the maximum tuning amplitude decreases as the underlying thin layer increases in thickness. However, given any one of the amplitude attribute plots, one would still not be able to distinguish which case it is.

Figures 9a to 9f are the corresponding instantaneous phase plots. In the zone of interest, there is virtually no visible difference among the various coloured phase plots, except for the last case (Fig. 9f) where the underlying thin layer is 25 m thick. Here, there is a visible green event (indicated by an arrow) where the phase plot curves slightly. Comparing this phase plot with the corresponding synthetic

seismogram in Figure 5f indicates that this phase effect comes from the tail end of the lower peak.

Figures 10a to 10f are the corresponding instantaneous frequency plots, and, by far, are the most revealing attribute. Since the instantaneous frequency is simply the time derivative of the instantaneous phase, any subtle change in the phase plot will be outlined even more clearly on the corresponding frequency plot. In the zone of interest, the six instantaneous frequency patterns all show significant differences. The first difference is that frequency tuning as reported by Robertson and Nogami (1984) is observed only in the 0 m and 5 m cases (Figs. 10a and 10b). The second difference is that the symmetrical pattern as shown in the 0 m case (Fig. 10a) gradually disintegrate into a completely non-symmetrical pattern for the 25 m case (Fig. 10f), with the six patterns all appearing significantly different from one another. These differences reflect the subtle waveform differences among the six models which are visually difficult to detect on conventional seismic data as well as on the other attribute plots.

CONCLUSION

In the last ten years or so, there has been a great deal of discussion on the use of AVO effects of P-wave to detect the presence of gas in clastic reservoirs. Ostrander's paper (1984) is an excellent example. However, there has not been much discussion on the effects of tuning on AVO effect. With the example shown in Figure 2 and Figure 3, we have demonstrated that tuning effects cannot be ignored if the bed thickness is below $(1/8)\,\lambda_d$. In the Western Canadian Sedimentary Basin, most clastic reservoirs are trapped in beds below $1/4\,\lambda_d$, many below $(1/8)\,\lambda_d$. To use AVO effect for exploring gas effectively, tuning effects must be taken into consideration. Furthermore, as demonstrated, the use of PS-wave AVO effects offer distinct advantages.

Another problem of interpreting data of clastic reservoirs from the Western Canadian Sedimentary Basin is that one often has to deal with a stack of many thin layers. It remains to be investigated how well the conclusions for one single thin bed could be applied to a stack of two layers or more. In the example we show, it is clear that visual interpretation could be very deceptive. Whenever possible, quantitative analysis such as trough to peak ratio should be performed. Also, the instantaneous frequency attribute seems to be most sensitive to subtle waveform changes. We plan to run several two-layer models and draw some useful conclusions by seeking some commonality among them.

ACKNOWLEDGEMENT

We would like to thank the support of the Crewes Project. We also thank Alberta Energy Company for assisting us in typing the manuscript and preparing the figures.

REFERENCES

Chung, H. and Lawton, D.C., 1990, AVO analysis and complex attributes for a Glauconitic gas sand bar, J. Can. Soc. Expl. Geophs. 26, 72-86.

de Voogd, N. and den Rooijen, H., 1983, Thin-layer response and spectral bandwidth: Geophysics 48, 12-18.

Ensley, R.A., 1984, Comparison of P- and S-wave seismic data: A new method for detecting gas reservoirs: Geophysics 49, 1420-1431.

Gardner, G.H.F., Gardner, L.W. and Gregory, A.R., 1974, Formation velocity and density - the diagnostic basics for stratigraphic traps: Geophysics 39, 770-780.

Gochioco, L.M., 1991, Tuning effect and interference reflections from thin beds and coal seams: Geophysics 56, 1288-1295.

Jain, S., 1987, Amplitude-vs-Offset analysis: A review with reference to application in Western Canada: J. Can. Soc. Expl. Geophys. 23, 27-36.

Kallweit, R.S. and Wood, L.C., 1982, The limits of zero-phase wavelets: Geophysics 47, 1035-1046.

Koefoed, O. and de Voogd, N., 1980, The linear properties of thin layers, with an application to synthetic seismograms over coal seams: Geophysics 45, 1254-1268.

Lange, J.N. and Almoghrabi, 1988, Lithology discrimination for thin layers using wavelet signal parameters: Geophysics 53, 1512-1519.

McCormack, M.D., et al., 1984, A case study of stratigraphic interpretation using shear and compressional seismic data: Geophysics 49, 509-520.

Meissner, R. and Meixner, E., 1969, Deformation of seismic wavelets by thin layers and layered boundary: Geophys. Prosp. 17, 1-27.

Ostrander, W.J., 1984, Plane-wave reflection coefficients for gas sands at non-normal angles of incidence: Geophysics 49, 1637-1648.

Robertson, J.D. and Nogami, H.H., 1984, Complex seismic trace analysis of thin beds: Geophysics 49, 344-352.

Robertson, J.D. and Pritchett, W.C., 1985, Direct hydrocarbon detection using comparative P-wave and S-wave seismic sections: Geophysics 50, 383-393.

Taner, M.T. and Sheriff, R.E., 1977, Applications of amplitude, frequency and other attributes to stratigraphic and hydrocarbon determination: AAPG Memoir 26, 301-327.

Taner, M.T., Koehler, F. and Sheriff, R.E., 1979, Complex seismic trace analysis: Geophysics 44, 1041-1063.

Widess, M.B., 1973, How thin is a thin bed?: Geophysics 38, 1176-1180.

Wren, A.E., 1984, Seismic techniques in Cardium exploration: J. Can. Soc. Expl. Geophys. 20, 55-59

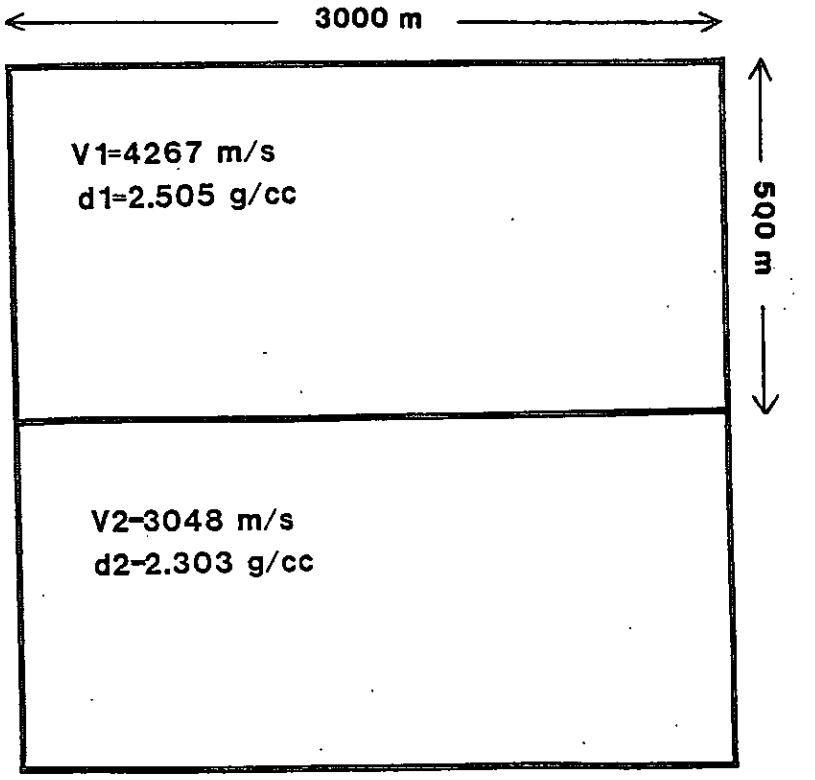

FIG. 1a. Model A, without tuning effect

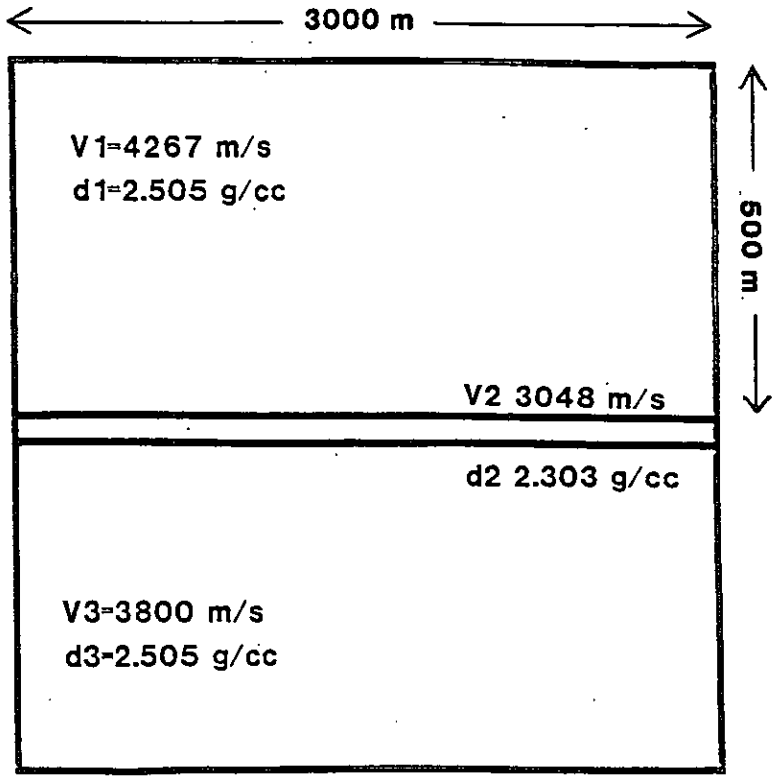

FIG. 1b. Model B, with tuning effect

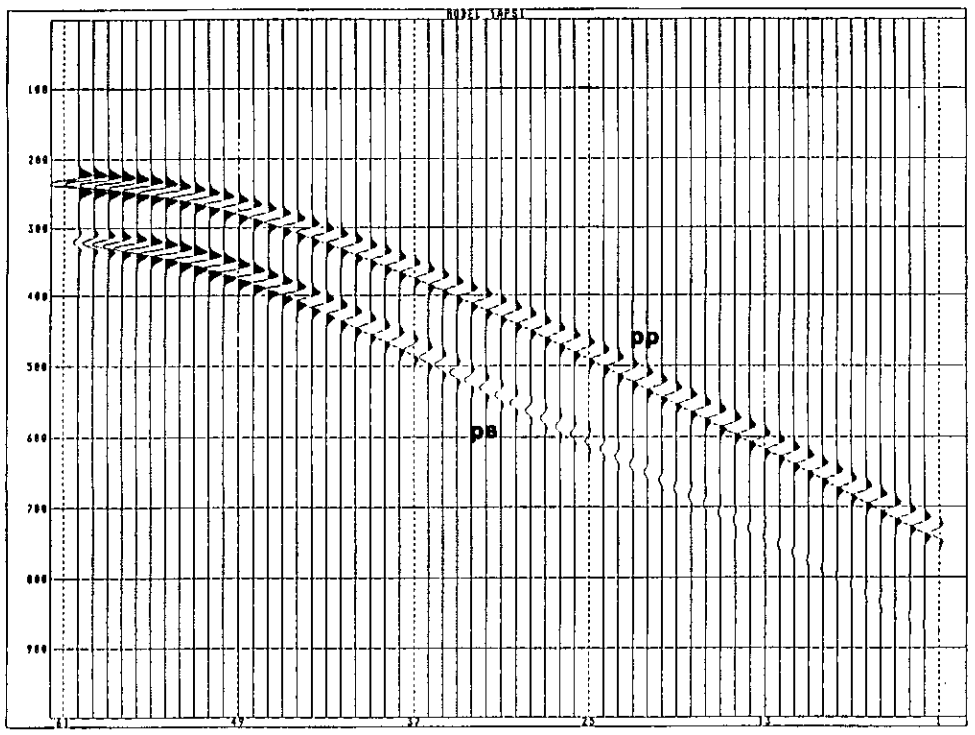

FIG. 2a. Synthetic seismogram for Model A, Poisson's ratio 0.1

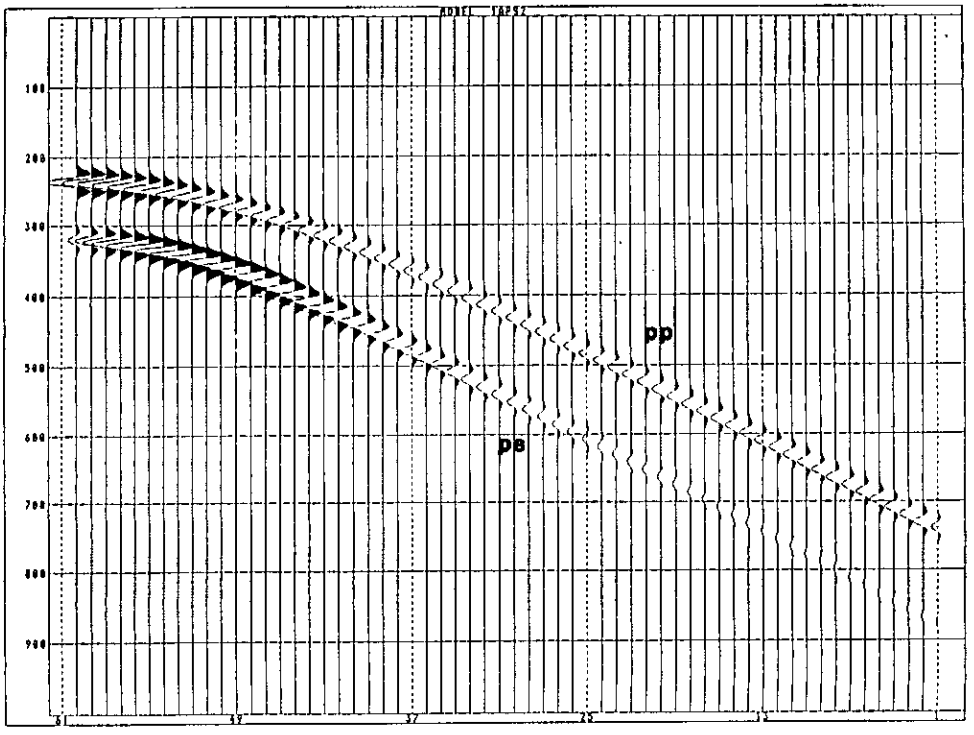

FIG. 2b. Synthetic seismogram for Model A, Poisson's ratio 0.25

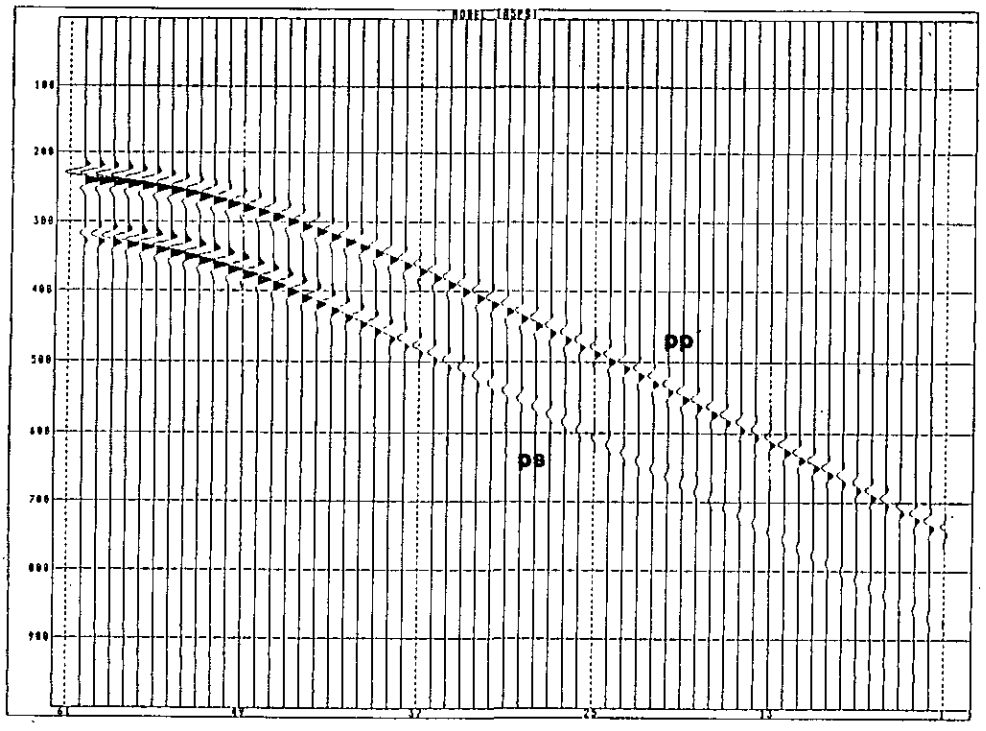

FIG. 2c. Synthetic seismogram for Model B, thickness 5 m, Poisson ratio 0.1

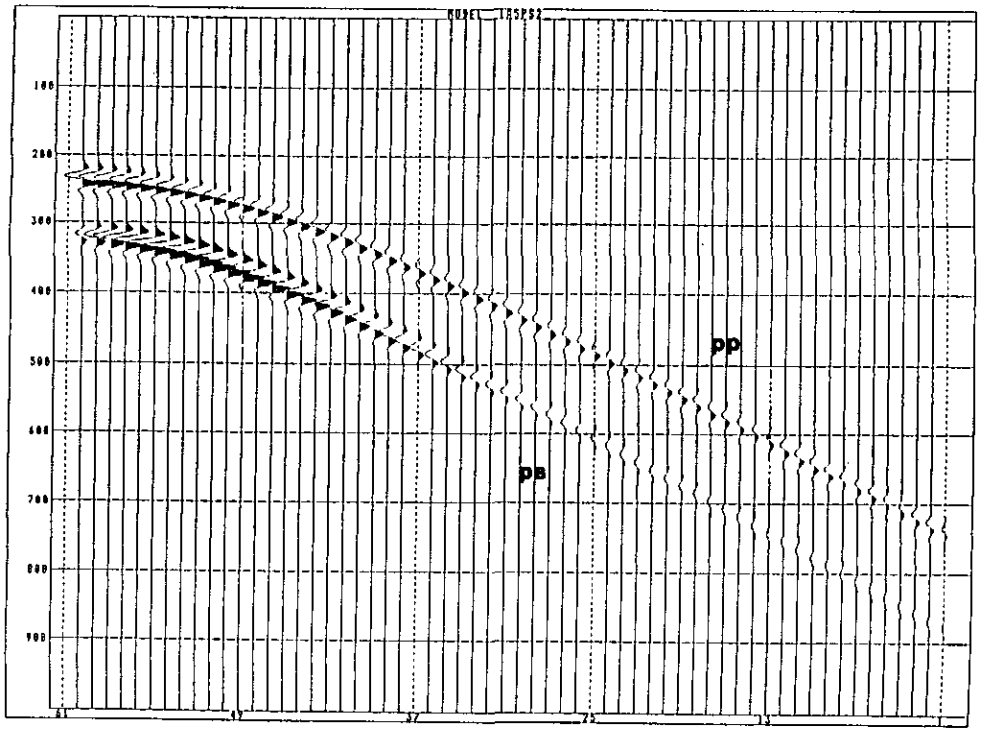

FIG. 2d. Synthetic seismogram for Model B, thickness 5 m, Poisson's ratio 0.25

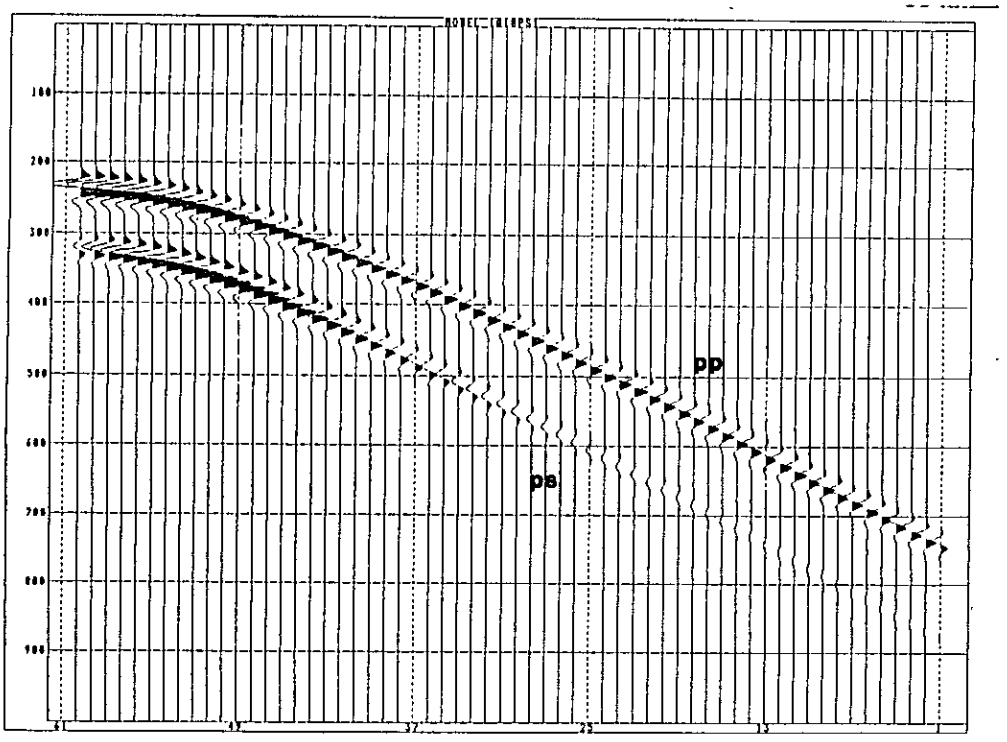

FIG. 2e. Synthetic seismogram for Model B, thickness 10 m, Poisson's ratio 0.1

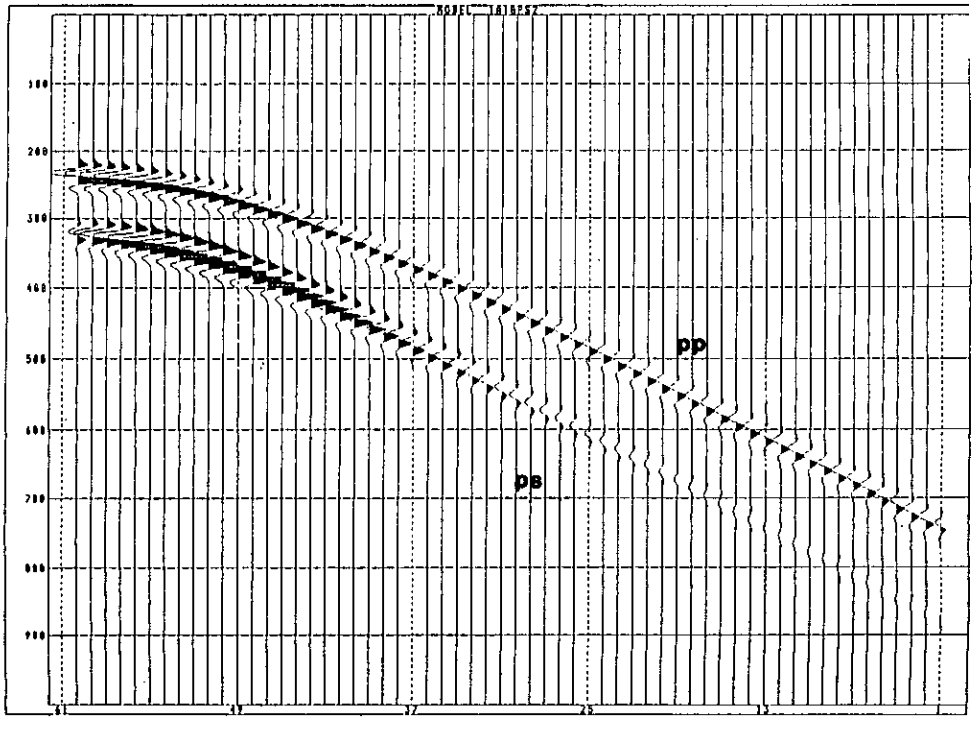

FIG. 2f. Synthetic seismogram for Model B, thickness 10 m, Poisson's ratio 0.25

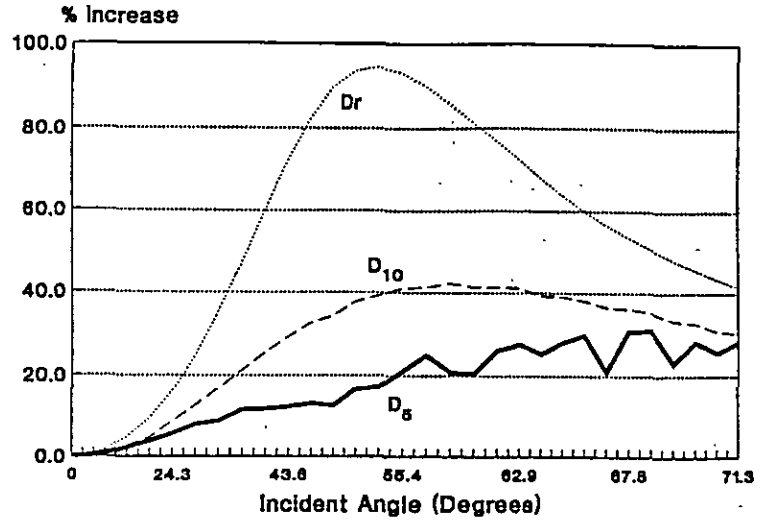

FIG. 3a. Tuning effects for P-wave reflections

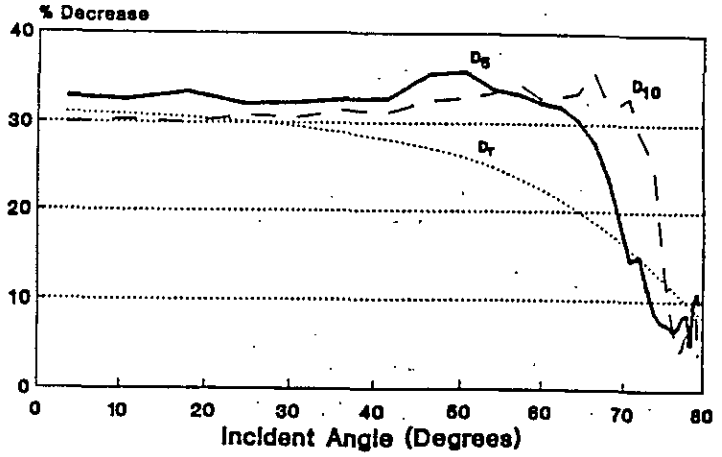

FIG. 3b. Tuning effects for PS-wave reflections

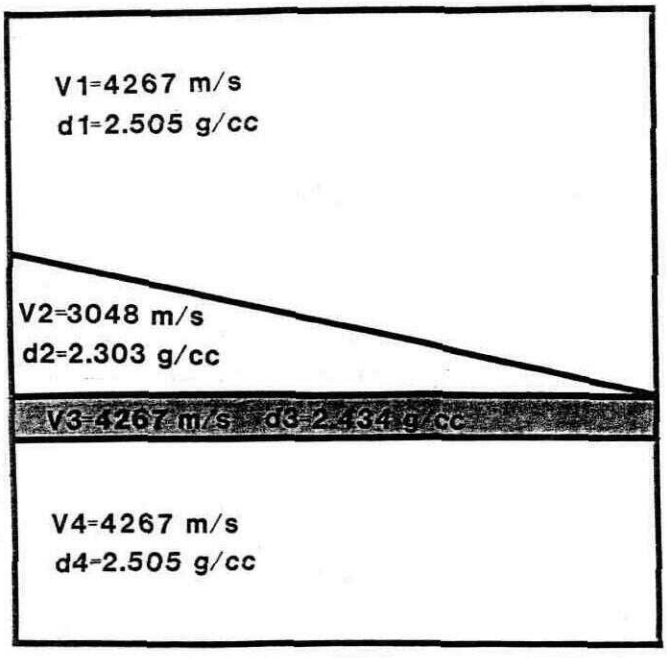

FIG. 4. Model for the two-layered study

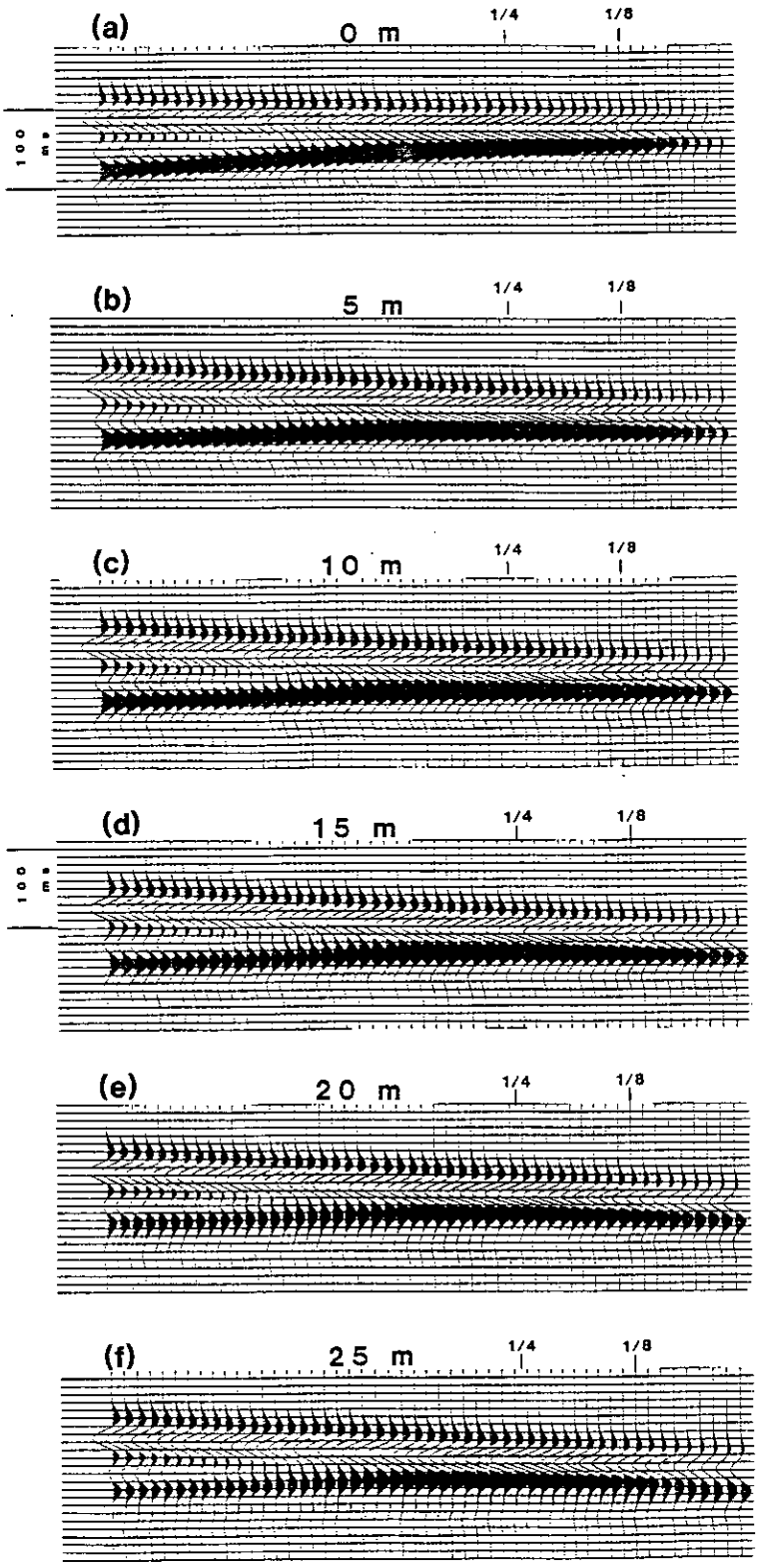

FIG. 5. Synthetic seismograms for the two-layered model

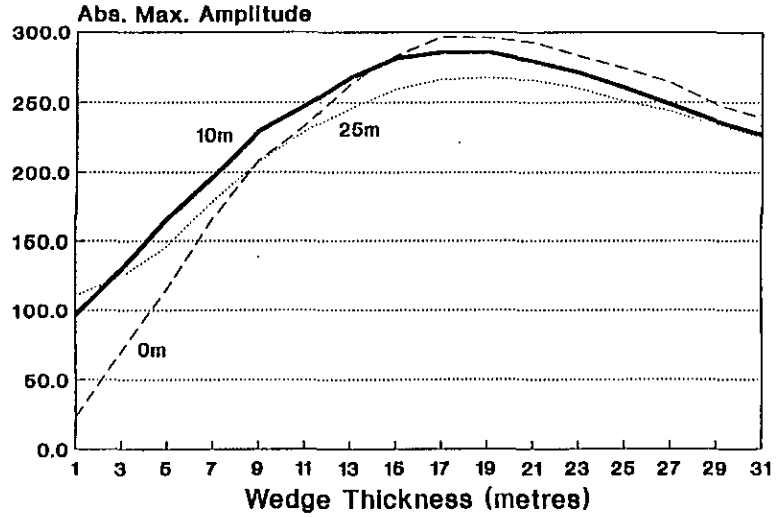

FIG. 6. Plots of absolute maximum amplitude versus the wedge thickness for the two-layered model

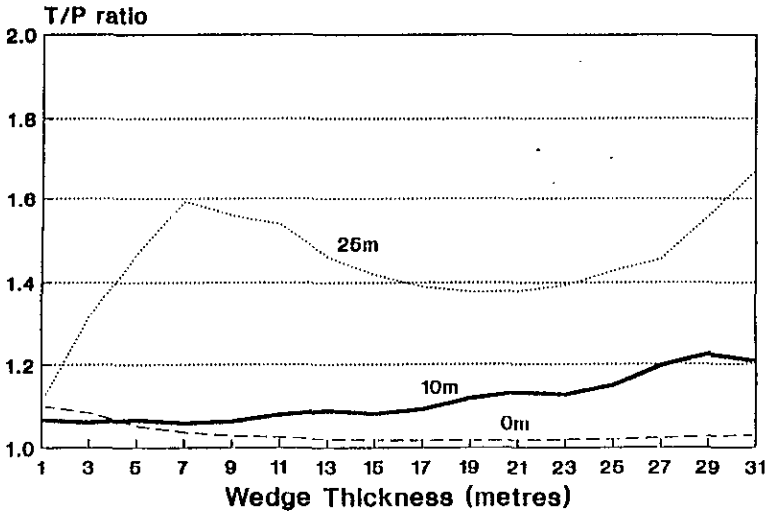

FIG. 7. Plots of the trough to peak ratio versus the wedge thickness for the two-layered model

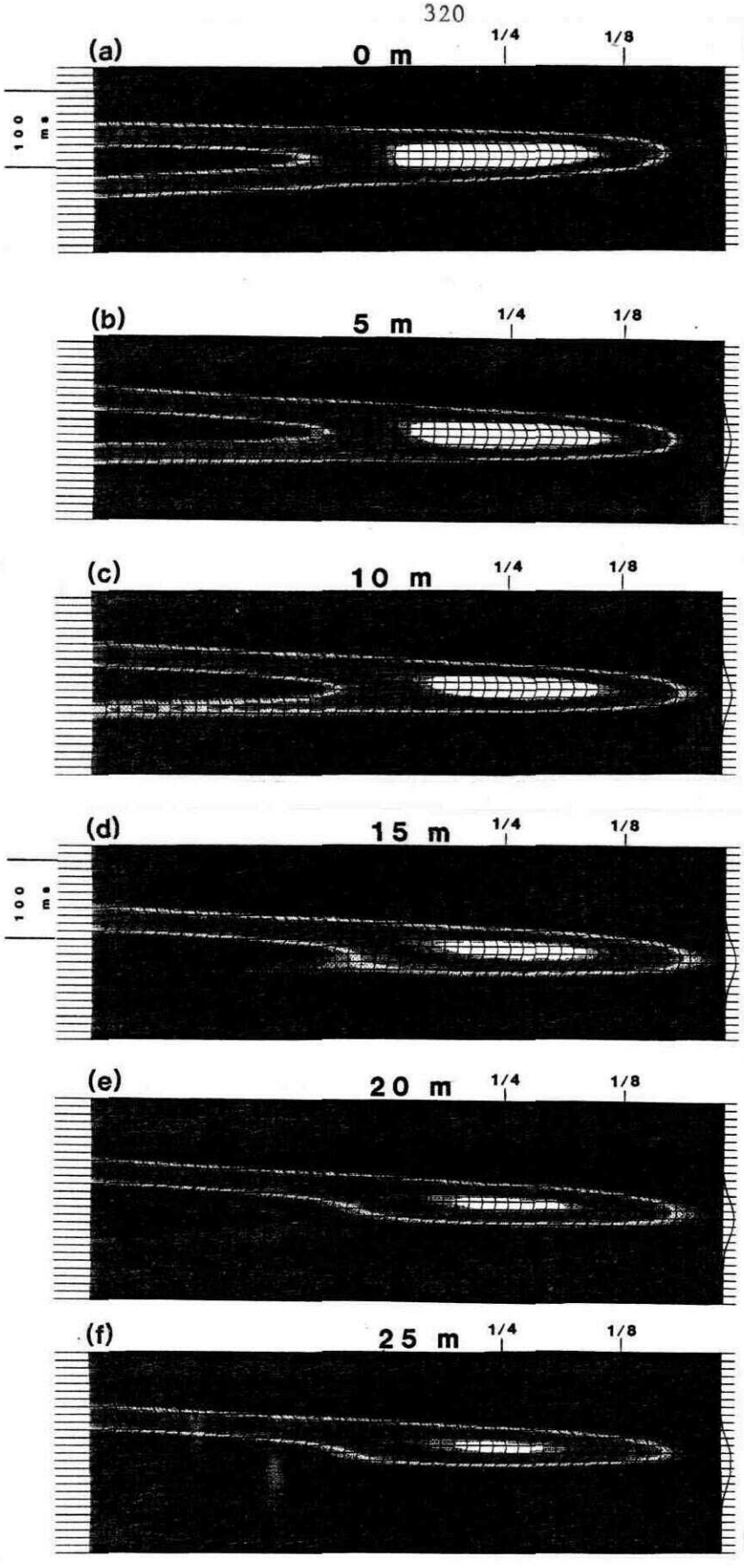

FIG. 8. Instantaneous amplitude plots for the two-layered model

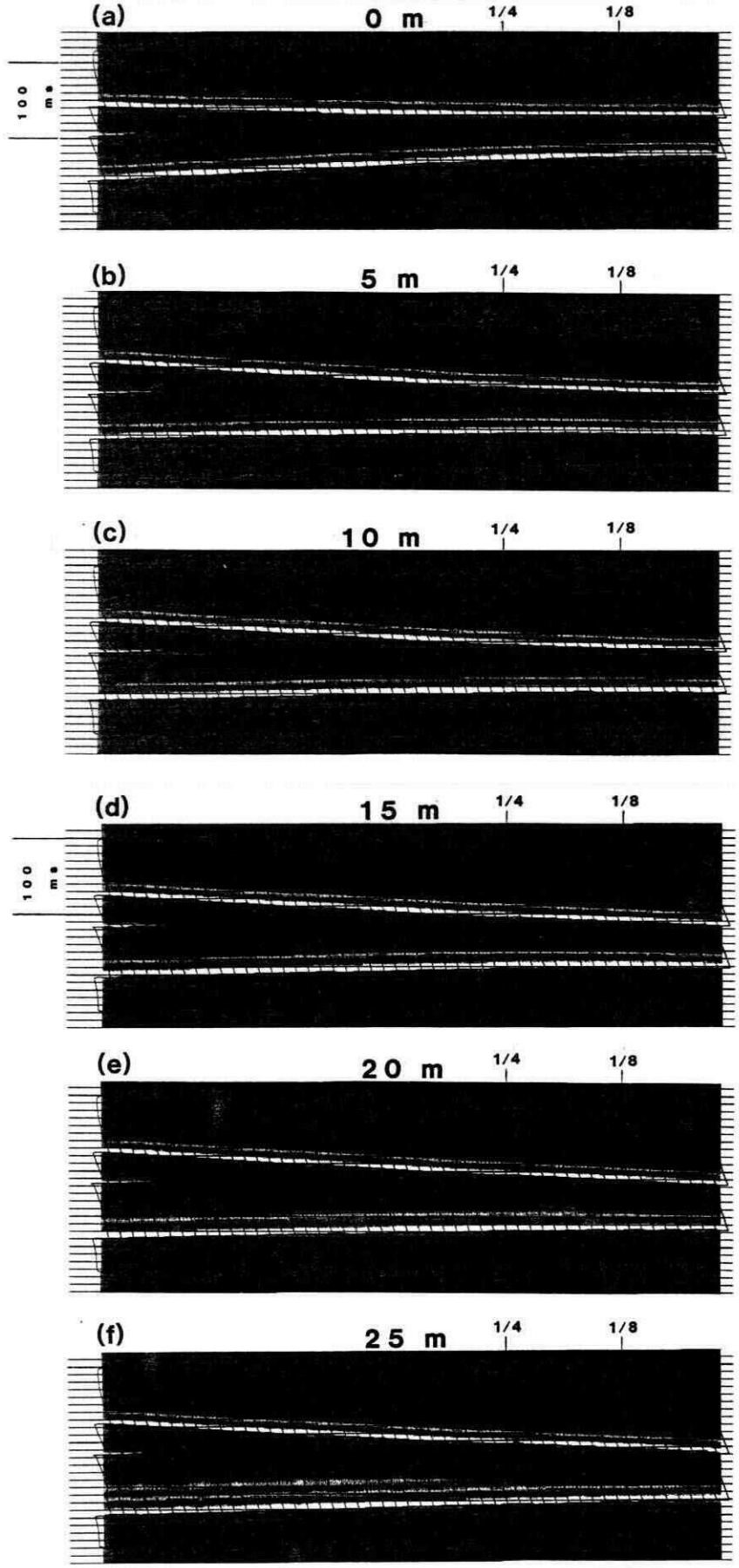

FIG. 9. Instantaneous phase plots for the two-layered model

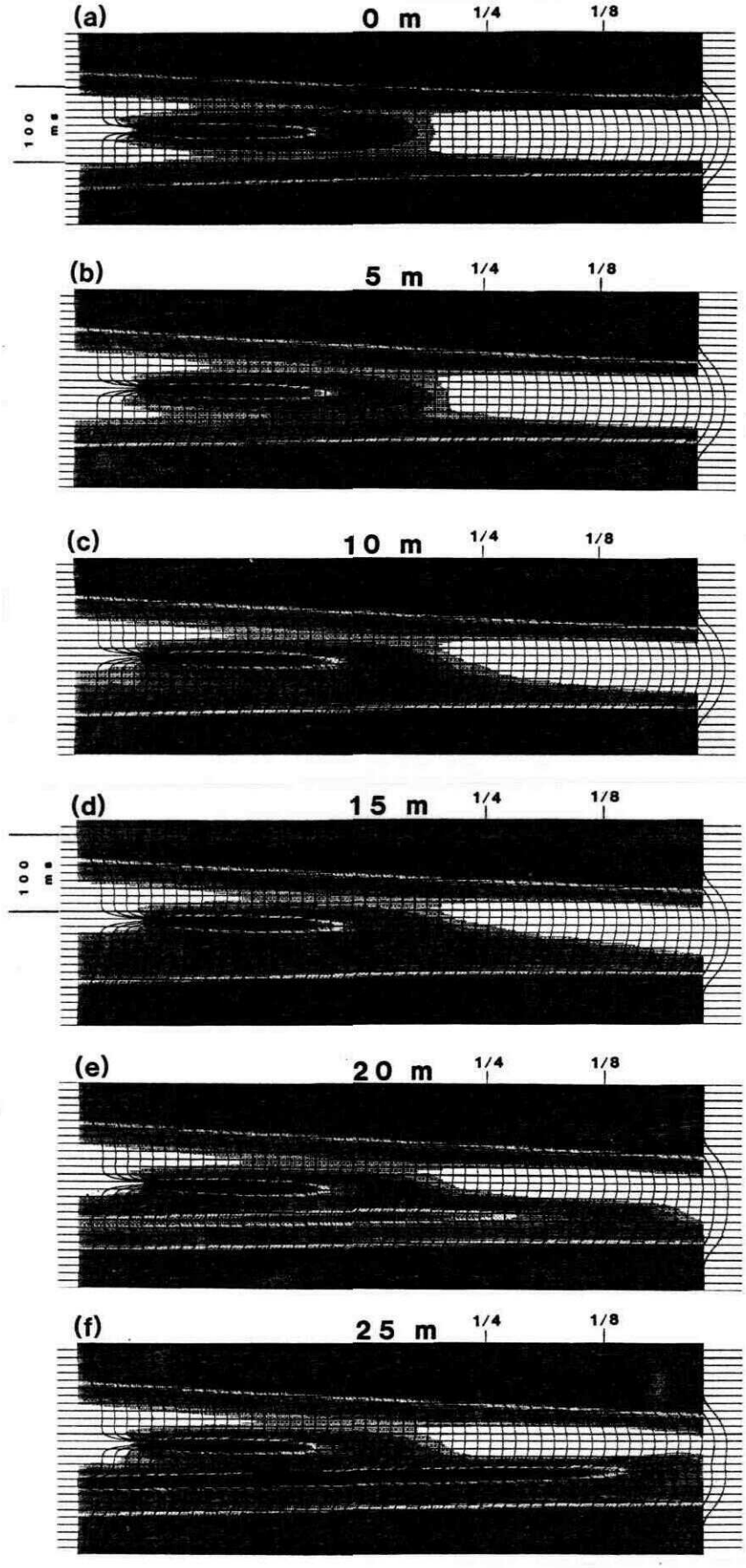

FIG. 10. Instantaneous frequency plots for the two-layered model